Tip-sample interaction force mediated by water molecules for AFM in water: Three-dimensional reference interaction site model theory

Masanori Harada*
Department of Nanoscience and Nanoengineering, Graduate School of Science and Engineering, Waseda University, 513 Waseda Tsurumaki-cho, Shinjuku-ku, Tokyo 162-0041, Japan

Masaru Tsukada
WPI-Advanced Institute for Materials Research, Tohoku University, 2-1-1 Katahira, Aobaku, Sendai 980-8577, Japan
(Received 6 November 2009; revised manuscript received 12 May 2010; published 13 July 2010)

Force curves and force maps of atomic force microscopy measurements for hypothetical nanostrucutres in aqueous environment have been simulated using the three-dimensional reference interaction site model (3D-RISM) theory. Various unexpected features of water mediated force are found including the directions of forces opposite to those in vacuum with local charges on both the tip and the sample. From those features and the density distributions of water around the peripheral of nanostructures obtained by the 3D-RISM theory, a close correlation has been found between the free energy of the system and the intactness of water density distributions around the tip and the sample surface. Moreover, it is shown that the 3D-RISM theory is much more precise for AFM simulations in water than the RISM theory from the fact that some of the important features cannot be described by the RISM theory.

DOI: 10.1103/PhysRevB.82.035414 PACS number(s): 07.79.Lh, 61.20.Ja, 68.37.Ps, 87.64.Dz

I. INTRODUCTION

Since its invention[1] the ability of atomic force microscopy (AFM) has been widely recognized and its application field has been extended remarkably. In AFM measurements in vacuum, it is not very difficult nowadays to obtain atomically resolved AFM images for inorganic crystal surfaces. Sugimoto and Oyabu have reported topographic noncontact AFM (NC-AFM) images of artificial atomic pattern of embedded Sn adatoms on a Ge(111)-c(2×8) surface.[2–4] This surface was made by manipulating single Sn atoms by the tip of AFM. Loppacher *et al.* have reported atomic resolution in topographic NC-AFM images of NaCl(001) and Cu(111).[5] However, the total force of the tip due to the sample is determined by complicated interplay of interactions, say, van der Waals interaction, electrostatic interaction, quantum mechanical orbital hybridization, atomic scale deformation both the sample and the tip side and so on. Therefore, it is not necessarily easy to understand what the measured quantity, from which the images is formed, represents.

For the above reasons, many theoretical simulations of AFM using models of a tip and a sample in vacuum have been performed so far. The mechanism to obtain the measured quantities and the underlying physics have been successfully explained in literatures.[6–14] Sasaki *et al.* have succeeded in visualizing theoretically the thermal fluctuation of the Si(111)-($\sqrt{3}\times\sqrt{3}$)-Ag surface at room temperature, and in reproducing the observed NC-AFM image.[10] We have succeeded in theoretically reproducing experimental NC-AFM images of 5-(4-methylthiophenyl)-10,15,20-tris(3,5-di-t-butylphenyl)porphyrin (MSTBPP) molecules and clarified experimental conditions for the observations.[14] More accurate and reliable simulations by means of density-functional theory (DFT) have been performed to explain the contrasts of NC-AFM images on ionic surfaces,[15–20] semiconductor surfaces,[21–24] and metal surfaces.[25] Moreover, the DFT simulation methods have also been able to explain the experimental results for atom identifications,[26] magnetic contrasts,[27] atom manipulations,[28–32] and energy dissipations.[33]

Recently, because of the improvement of experimental methods for AFM,[34,35] data with atomic scale resolution can be obtained not only in vacuum but also in water. Images with molecular resolution of a crystal surface of polydiacetylene molecules in water[36] and images with atomic resolution of a cleaved (001) surface of muscovite mica in water have been successfully recorded with NC-AFM using small oscillation amplitude by Fukuma *et al.*[37] Precise controls of the interaction forces between a tip and bacteriorhodopsins in water have been demonstrated by Hoogenboom *et al.*[38] They have imaged a peptide loop between two transmembrane helices of a bacteriorhodopsin and have deliberately bended it with the precise controls of the forces. However, effective theoretical methods for AFM simulation in water have not been established so far. If the gap between the AFM experiments and the theoretical simulations is filled, new fields of AFM application will be much expanded and accelerated.

In AFM measurement in liquids, liquid molecules mediate the force between a tip and a sample. The motions of the liquid molecules are random and much more rapid[39–41] compared to the tip motion.[36–38] The rapid random motions of the liquid molecules affect the force felt by the tip and should be included in AFM simulations for models in liquids. For simulations of AFM for samples in vacuum, positions of individual atoms of a tip or a sample can be calculated by the conjugate gradient (CG) method[42] and a force is obtained for the determined atomic structure. However, the rapid random motions of a large number of liquid molecules preclude such a kind of simple mechanical calculations. New methods incorporating the effect of the rapid random motions of liquid molecules are required.

The method where a liquid is modeled by a continuum dielectric medium[43,44] is conceivable. However, such a

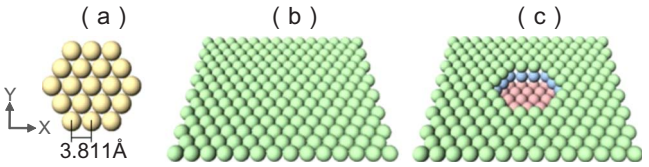

FIG. 1. (Color online) (a): top view of the tip structure, (b): plane surface, and (c): pit surface.

model cannot represent the atomic scale behavior of the liquid and is not suitable for AFM simulations. Another possible methodology of AFM simulation to include the effect of liquid molecules is the molecular dynamics (MD) method.[45–49] The motions of individual liquid molecules are calculated as they are in experimental environments. However, the method is unrealistic from the view point of calculation cost; the numbers of the water molecules are so large and the speeds of individual molecules are extremely fast compared to the motion of the tip.

To overcome this difficulty, Koga *et al.* used a statistical method of liquid solutions called reference interaction site model (RISM) theory[50–55] for contact mode AFM simulations using an artificial model of a tip and a sample.[56–58] The RISM theory is a theory of liquid solutions based on the statistical mechanics and can treat the ensemble averages of behaviors of liquid molecules. Namely, the time scale and the size treated by the RISM theory are appropriate for the description of physical properties represented by AFM data. Moreover, the RISM theory has an advantage of much lower computational cost, which is impossible by the all-atom MD simulations. On the other hand, it has an advantage of providing atomic scale information, which cannot be obtained by the continuum model. In the RISM theory, density-density correlation functions between the atoms of liquids and atoms of a tip or a sample are obtained as functions of distances between the atoms. These correlation functions are used to calculate water mediated forces for AFM simulations.

The three-dimensional RISM (3D-RISM) theory[50,59–64] is more precise than the RISM theory. In the 3D-RISM theory, density distributions of atoms of liquids around a tip and samples are obtained as functions of three-dimensional real space coordinates and are used to calculate water mediated forces for AFM simulations. The RISM theory is not precise compared with the 3D-RISM theory, because in the RISM theory, the density distributions are only indirectly obtained by superposing the density-density correlation functions and the obtained density distributions are not precise since the density-density correlation functions are treated only as functions of the distances between atoms and not the functions of the relative three-dimensional space coordinates. The density distributions of liquid atoms around a tip and a sample are useful to discuss effects of the liquids on the simulated forces.

We report in the present paper the application of the 3D-RISM theory for the AFM simulations in aqueous environment. Force curves and force maps for hypothetical nanostrucutres in water are simulated using the 3D-RISM theory. Features of the force curves and the force maps are extracted and compared with those obtained by the RISM theory. We will find remarkable changes of the tip-sample interaction force caused due to the water molecules, and their mechanisms are clarified in the present paper. An important clue is obtained by the density distributions of the oxygen atoms and the hydrogen atoms in water around the peripherals of the nanostructures. The features of the force curves and the force maps are explained using the density distributions.

In Sec. II, the structures of the model systems, and the potential parameters, are described as well as the simulation methods using the RISM theory and the 3D-RISM theory. In Sec. III, the results of simulation for the force curves and the force maps by the 3D-RISM theory are reported and compared with those obtained by the RISM theory. The difference of the force curves between in water and in vacuum is compared; the latter is used as a reference. Interesting phenomenon we found is that the direction of forces in water can be opposite to that in vacuum; this is particularly seen for the tip and the surface with localized charge distribution. In Sec. IV, to discuss the results of the simulated forces, the density distributions of water molecules around the tip only and those around the sample surface only are obtained by the 3D-RISM theory. The unexpected features of the forces leading to the interesting phenomena are explained based on the relation of the free energy of the system with the overlap of the water density distributions.

II. MODELS AND CALCULATION METHODS

A. Models

The purpose of the AFM simulations performed in this paper is to reveal general features of the AFM measurements in water not sticking to a specific experimental result. The structures of the tip and the samples used in the simulations

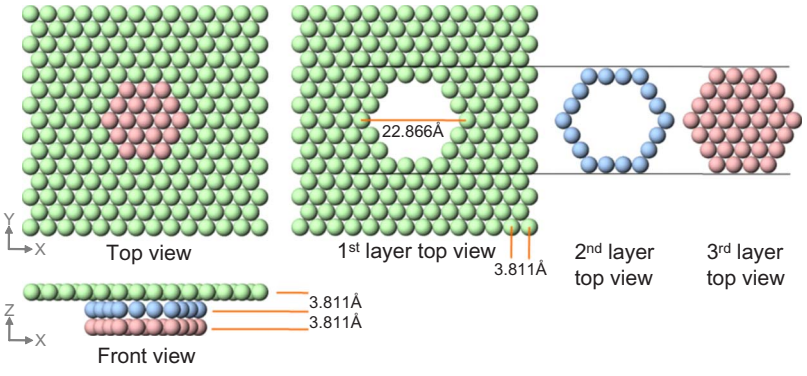

FIG. 2. (Color online) The detailed structures of the pit surface.

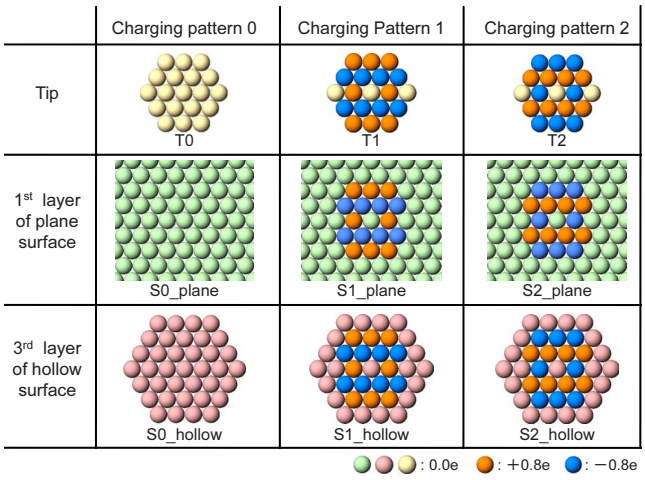

FIG. 3. (Color online) Three types of the charging pattern 0, 1, and 2.

are simple and somewhat hypothetical to avoid unessential complications and to save unnecessary calculation cost.

The tip is modeled as a sixfold rotationally symmetric monolayer made up of 19 hypothetical atoms as shown in Fig. 1(a). The distance between two neighboring atoms is 3.811 Å.

Though the tip shape is not realistic, flat geometries are preferable to other realistic structure such as a pyramidal structure in order to qualitatively investigate the effect of the water molecules between the tip and the surface because the flat tip contacts more water molecules than the other candidates. Furthermore, a larger tip volume increases the direct interaction between the tip and a surface which are not the interactions investigated in this report. Two types of surface structures are modeled. A plane surface is modeled as shown in Fig. 1(b), which is made up of 203 hypothetical atoms. More complicated structures should be investigated to clarify the ability of the 3D-RISM theory to obtain density distributions of water. The surface with a pit (hereafter called as pit surface) is modeled as shown in Fig. 1(c) which is made up of 239 hypothetical atoms. The detailed structure of the pit surface, which is constructed of three layers, is shown in Fig. 2. The distances between two neighboring layers are 3.811 Å. The distances between two neighboring atoms, which are in the same layer are also 3.811 Å.

Density distribution of water molecules around the boundary of the sample surface is expected to depend strongly on electric charging states of individual atoms of the surface because of the significant polarization of water molecule. We introduce three types of charging pattern, 0, 1, and 2 for both the tip and the sample surface as shown in Fig. 3. The structures forming the three charging patterns are made of three types of hypothetical atoms, namely, positively charged atom, negatively charged atom and neutral atom. The electric charges of the positively charged and the negatively charged atoms are 0.8 and −0.8 times the elementary charge, respectively. All atoms of charging pattern 0 are neutral atoms. Charging pattern 1 is constructed of 8 positively charged atoms, 8 negatively charged atoms and remaining neutral atoms. Individual atom charges of charging pattern 2 are just opposite in sign to those of charging pattern 1.

For later convenience, the following naming rules are adopted to describe the charging patterns and structures. "T" and "S" represent the tip and the sample surface, respectively. "0," "1." or "2" following T or S represents the charging pattern of the tip or the sample surface, respectively. "_plane" or "_pit" following "S0," "S1," or "S2" represents the structure of the sample surface. For example "T0S2_pit" means the tip with charging pattern 0 and the surface with a pit (called pit surface hereafter) with charging pattern 2. "S0_pit" means the pit surface with charging pattern 0.

B. Potentials

We use the similar potential model as the theoretical simulation by Koga *et al.*[56–58] TIPS site-site interaction potential by Jorgensen[65] is used for the interaction between two water molecules $V_{W_A W_B}$. Namely, the interaction between two water molecules W_A and W_B is calculated as the sum of electrostatic interactions and Lennard-Jones interactions for all pairs of two atoms of W_A and W_B as follows:

$$V_{W_A W_B} = \sum_{a}^{\text{in } W_A} \sum_{b}^{\text{in } W_B} \left(\frac{q_a q_b e^2}{r_{ab}} + \frac{A_{ab}}{r_{ab}^{12}} - \frac{C_{ab}}{r_{ab}^{6}} \right), \quad (e^2 = 332 \text{ kcal Å/mol}), \tag{1}$$

where r_{ab} is the distance between atom a and b. The quantities q_a and q_b are the electric charges of atoms a and b, respectively. For the case of water molecule, by the unit of the elementary electric charge −0.8 and 0.4 are assigned for the oxygen atom and the hydrogen atom, respectively. The parameters A_{ab} and C_{ab} depend on the combination of the atoms as shown in Table I. The numerical value of A_{OH} is different from the value by Jogensen which is 0. The introduction of small nonzero value for A_{OH} is to avoid overlap of the opposite site charges which causes the divergence of the RISM calculation. The value of A_{OH} is the same as the one used by the Pettitt *et al.*[66] for the same reason.

The potential for the tip-sample interaction V_{TS}, that for the tip-water interaction V_{TW} and that for the surface-water interaction V_{SW} are calculated respectively as the sum of Lennard-Jones interaction energies and electrostatic interaction energies as follows:

TABLE I. Lennard-Jones parameters of TIPS water. O and H of subscripts represent oxygen and hydrogen atoms, respectively. The unit of A_{ab} and C_{ab} are kcal Å^{12}/mol and kcal Å^{6}/mol, respectively.

A_{OO}	A_{OH}	A_{HH}	C_{OO}	C_{OH}	C_{HH}
58000	225.180	0.0	525.000	0.0	0.0

TABLE II. Lennard-Jones potential parameters and electric charges for interactions V_{TS}, V_{TW}, and V_{SW}.

	Neutral atom	Positive atom	Negative atom	Hydrogen atom	Oxygen atom
ϵ_i(eV)	0.00578	0.00578	0.00578	0.001	0.005151
σ_i(Å)	3.395	3.395	3.395	0.001	3.215
q_i	0	+0.8	−0.8	+0.4	−0.8

$$V_{AB} = \sum_{a}^{\text{in } A} \sum_{b}^{\text{in } B} \left\{ 4\epsilon_{ab} \left[\left(\frac{\sigma_{ab}}{r_{ab}} \right)^{12} - \left(\frac{\sigma_{ab}}{r_{ab}} \right)^{6} \right] + \frac{q_a q_b e^2}{r_{ab}} \right\}$$

$$\left(\begin{array}{l} e^2 = 332 \text{ kcal Å/mol}, \\ AB = TS, \ TW \quad \text{or} \quad SW \end{array} \right). \tag{2}$$

Here ϵ_{ab} and σ_{ab} are determined by combining rules $\epsilon_{ab} = \sqrt{\epsilon_a \epsilon_b}$ and $\sigma_{ab} = (\sigma_a + \sigma_b)/2$ where ϵ_i and σ_i are assigned for each atom i. Parameters ϵ_i, σ_i and q_i for the three types of atoms constructing the tips and the surfaces and the hydrogen and the oxygen atom of water are listed in Table II.

The direct force between a tip and a surface in the z direction is calculated by differentiating the direct interaction between the tip and the surface, V_{TS} with respect to a tip height. The water mediated force is calculated by the RISM theory or the 3D-RISM theory as explained in the next subsection. The direct force and the water mediated force are calculated individually and summed up to obtain the total force between the tip and the surface in water.

C. RISM and 3D-RISM theories for AFM simulations

The essence of the RISM theory can be expressed by the following simultaneous matrix equations, i.e., the site-site Ornstein-Zernike (SSOZ) equation, Eq. (3), and the hypernetted chain (HNC) equation, Eq. (4):

$$h_{\alpha\gamma}(r) = \sum_{\mu,\nu=1}^{N} [w_{\alpha\mu}(r) * c_{\mu\nu}(r) * w_{\nu\gamma}(r) + w_{\alpha\mu}(r) * c_{\mu\nu}(r) * \rho_{\nu\nu} h_{\nu\gamma}(r)], \tag{3}$$

$$c_{\alpha\gamma}(r) = \exp[-\beta\phi_{\alpha\gamma}(r) + t_{\alpha\gamma}(r)] - 1 - t_{\alpha\gamma}(r)$$

$$[t_{\alpha\gamma}(r) \equiv h_{\alpha\gamma}(r) - c_{\alpha\gamma}(r)]. \tag{4}$$

Here, $\beta = 1/k_B T$ with the Boltzmann constant k_B and the temperature T. The functions $h_{\alpha\gamma}(r)$, $w_{\alpha\gamma}(r)$, $c_{\alpha\gamma}(r)$ and $\phi_{\alpha\gamma}(r)$ are the (α, γ) matrix elements of $N \times N$ symmetrical matrices where r is the distance between two atoms α and γ and N is the sum of the numbers of the in-equivalent atoms constituting both the solute molecular species and the solvent molecular species; $h_{\alpha\gamma}(r)$ and $c_{\alpha\gamma}(r)$ are the total and direct correlation functions between two atoms α and γ. $w_{\alpha\gamma}(r)$ is the correlation function between the two atoms α and γ belonging to the same molecule. $\phi_{\alpha\gamma}(r)$ is the direct interaction between two atoms α and γ in vacuum. The quantity $\rho_{\alpha\alpha}$ is the (α, α) matrix element of a $N \times N$ diagonal matrix and means number density of the atom α. The symbol $*$ means a convolution integral with respect to r.

The combined system of a tip and a surface in water is treated as a single solute molecule in an infinitely dilute liquid solution by the RISM theory. By substituting 0 for $\rho_{\nu\nu}$ for the atoms of the tip and the surface, Eqs. (3) and (4) can be transformed into the following equations:

$$h^{VV}_{\alpha\gamma}(r) = \sum_{\mu,\nu=1}^{N_V} [w^{VV}_{\alpha\mu}(r) * c^{VV}_{\mu\nu}(r) * w^{VV}_{\nu\gamma}(r) + w^{VV}_{\alpha\mu}(r) * c^{VV}_{\mu\nu}(r) * \rho^{VV}_{\nu\nu} h^{VV}_{\nu\gamma}(r)], \tag{5}$$

$$c^{VV}_{\alpha\gamma}(r) = \exp[-\beta\phi^{VV}_{\alpha\gamma}(r) + t^{VV}_{\alpha\gamma}(r)] - 1 - t^{VV}_{\alpha\gamma}(r)$$

$$[t^{VV}_{\alpha\gamma}(r) \equiv h^{VV}_{\alpha\gamma}(r) - c^{VV}_{\alpha\gamma}(r)], \tag{6}$$

$$h^{UV}_{\alpha\gamma}(r) = \sum_{\mu=1}^{N_U} \sum_{\nu=1}^{N_V} [w^{UU}_{\alpha\mu}(r) * c^{UV}_{\mu\nu}(r) * w^{VV}_{\nu\gamma}(r) + w^{UU}_{\alpha\mu}(r) * c^{UV}_{\mu\nu}(r) * \rho^{VV}_{\nu\nu} h^{VV}_{\nu\gamma}(r)], \tag{7}$$

$$c^{UV}_{\alpha\gamma}(r) = \exp[-\beta\phi^{UV}_{\alpha\gamma}(r) + t^{UV}_{\alpha\gamma}(r)] - 1 - t^{UV}_{\alpha\gamma}(r)$$

$$[t^{UV}_{\alpha\gamma}(r) \equiv h^{UV}_{\alpha\gamma}(r) - c^{UV}_{\alpha\gamma}(r)], \tag{8}$$

TABLE III. Data sampling on logarithmic radial coordinate.

	RISM	RISM	3D-RISM
	solvent-solvent Eqs. (5) and (6)	solvent-solute Eqs. (7) and (8)	solvent-solvent Eqs. (5) and (6)
Upper range	1.123×10^3 Å		8.680×10^3 Å
Lower range	2.445×10^{-4} Å		3.162×10^{-3} Å
N sampling	768		512

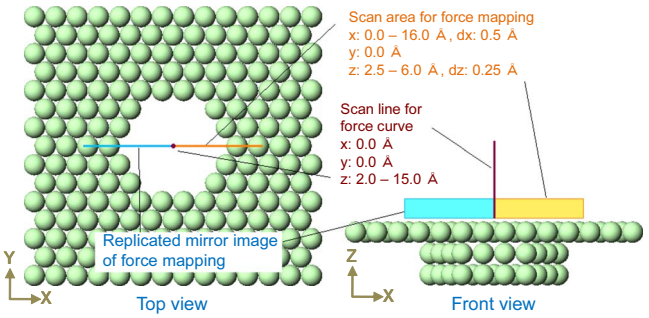

FIG. 4. (Color online) The purple line indicates the scan line for the simulation of force-distance curve. For the simulation of x-z plane force map, forces are calculated in the yellow colored area to form a force map. The calculated force map is replicated in the blue colored area to obtain its mirror image.

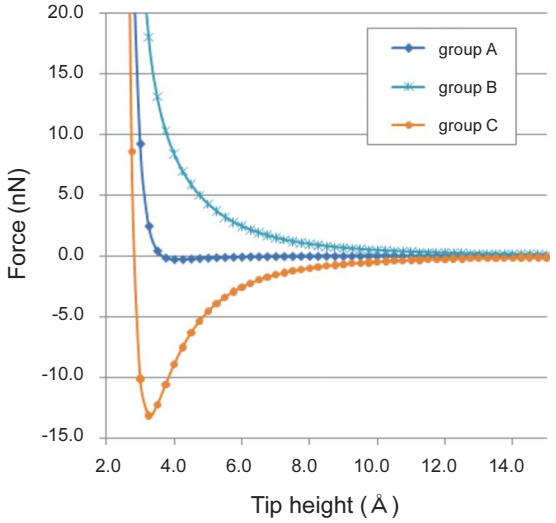

FIG. 5. (Color online) Force curves corresponding to the direct interactions between the tip and the surface in vacuum. Group A interact by the Lennard-Jones (L-J) potentials, group B interact by the L-J and repulsive electrostatic potentials and group C interact by the L-J and attractive electrostatic potentials.

where V and U represent the solvent and the solute, respectively. N_V and N_U are the numbers of the atoms constituting the solvent molecular species and the solute molecular species, respectively. The radial total correlation functions of the pure solvent, $h_{\alpha\beta}^{VV}(r)$, obtained first by Eqs. (5) and (6) are substituted in Eq. (7). Then $h_{\alpha\gamma}^{UV}(r)$ for solute atom α and solvent atom γ is obtained by Eqs. (7) and (8).

The major part of the 3D-RISM theory for an infinitely dilute liquid solution can be expressed by the following simultaneous equations,[50] i.e., the Ornstein-Zernike (OZ) equation, Eq. (9), and the Kovalenko-Hirata (KH) equation,[62,64] Eq. (10):

$$h_\gamma^{UV}(x,y,z) = \sum_{\nu=1}^{N_V} [c_\nu^{UV}(x,y,z) * w_{\nu\gamma}^{VV}(r) + c_\nu^{UV}(x,y,z) * \rho_{\nu\nu}^{VV} h_{\nu\gamma}^{VV}(r)], \tag{9}$$

$$c_\gamma^{UV}(x,y,z) = \begin{cases} \exp[d_\gamma^{UV}(x,y,z)] - 1 - t_\gamma^{UV}(x,y,z) & \text{for} \quad d_\gamma^{UV}(x,y,z) \le 0 \\ d_\gamma^{UV}(x,y,z) - t_\gamma^{UV}(x,y,z) & \text{for} \quad d_\gamma^{UV}(x,y,z) > 0 \end{cases},$$

$$\left[\begin{array}{c} d_\gamma^{UV}(x,y,z) \equiv -\beta\phi_\gamma^{UV}(x,y,z) + t_\gamma^{UV}(x,y,z), \\ t_\gamma^{UV}(x,y,z) \equiv h_\gamma^{UV}(x,y,z) - c_\gamma^{UV}(x,y,z) \end{array} \right]. \tag{10}$$

Here, like the RISM theory, the radial total correlation functions of the pure solvent, $h_{\alpha\beta}^{VV}(r)$, obtained first by Eqs. (5) and (6) are substituted in Eq. (9). The functions $h_\alpha^{UV}(x,y,z)$, $c_\alpha^{UV}(x,y,z)$ and $\phi_\alpha^{UV}(x,y,z)$ are the αth elements of $1 \times N_V$ row vectors, depending on the x, y, and z coordinates of atom α in the three-dimensional real space. $\rho_{\nu\nu}^{VV}$ is the number density of the water molecules of pure water and the same constant value at all positions in the simulation cell. The three-dimensional correlation function, $h_\alpha^{UV}(x,y,z)$, corresponds to the density of atom α at position (x,y,z) by the relation $\rho_0[h_\alpha^{UV}(x,y,z)+1]$ where ρ_0 is the density of pure water. Equations (9) and (10) are solved iterative scheme starting from $h_\alpha^{UV}(x,y,z)=0$ at all positions which are the same value for the pure water. For numerical calculations of Eqs. (5)–(8), numerical data are sampled at evenly spaced points in a range of logarithmic radial coordinates. The ranges and the numbers of the sampling for our calculations are shown in Table III.

For numerical calculations of Eqs. (9) and (10), numerical data are sampled at grid points in a volume. For our calculations, the lengths of the volume in the x, y, and z directions are 54, 54, and 80 Å, respectively, and the grid spacing is 0.25 Å. The volume is sufficiently large to contain the entire system of the tip and the sample. The periodic boundary condition and the cutoff radius of 37.5 Å are used to calculate the electrostatic potentials at the grid points. For Lennard-Jones potentials, neither a cutoff radius nor the periodic boundary condition is used. Namely, the electrostatic part of the potential field is calculated by summing up the potential energies between solvent atom α and the atoms of the tip and surface in the simulation cell and periodic copied tips and surfaces in 26 neighboring cells in the condition that the distance between the atom α and a tip atom or a surface

atom is less than 37.5 Å. The Lennard-Jones part of the potential field is calculated by summing up the potential energies between the atom α and the tip and surface atoms only in the simulation cell without any distance conditions.

In the RISM theory, the free energy for tip height H, E_H, is calculated from the radial correlation functions, $h_{\alpha\gamma}^{UV}(r;H)$ and $c_{\alpha\gamma}^{UV}(r;H)$, obtained by solving the equations, (5)–(8) for the tip height of H as follows:

$$E_H = \sum_{\alpha}^{N_U}\sum_{\gamma}^{N_V}\left\{4\pi\rho_{\gamma\gamma}^{VV}k_BT\int_0^{\infty}drr^2\left[\frac{1}{2}h_{\alpha\gamma}^{UV}(r;H)h_{\alpha\gamma}^{UV}(r;H) - c_{\alpha\gamma}^{UV}(r;H) - \frac{1}{2}h_{\alpha\gamma}^{UV}(r;H)c_{\alpha\gamma}^{UV}(r;H)\right]\right\}. \quad (11)$$

Here the free energy means the relative value of the free energy of the system consisting of a tip and a sample surface in water compared to the sum of the free energy of the system consisting of the tip and the sample surface in vacuum and the total energy of the bulk water.

Similarly, in the 3D-RISM theory, the free energy of an entire system for tip height H, E_H, is calculated from the three-dimensional correlation functions, $h_{\gamma}^{UV}(x,y,z;H)$ and $c_{\gamma}^{UV}(x,y,z;H)$, obtained by solving the equations, Eqs. (5), (6), (9), and (10) for tip height H as follows:

$$E_H = \sum_{\gamma}^{N_V}\left\{\rho_{\gamma\gamma}^{VV}k_BT\int\int\int_0^{\infty}dxdydz\left\{\frac{1}{2}[h_{\gamma}^{UV}(x,y,z;H)]^2 \times \mathrm{U}[-h_{\gamma}^{UV}(x,y,z;H)] - c_{\gamma}^{UV}(x,y,z;H) - \frac{1}{2}h_{\gamma}^{UV}(x,y,z;H)c_{\gamma}^{UV}(x,y,z;H)\right\}\right\}, \quad (12)$$

where $\mathrm{U}(x)$ is the Heaviside unit step function defined as follows:

$$\mathrm{U}(x) = \begin{cases} 0, & x < 0 \\ 1, & x \geq 0 \end{cases}. \quad (13)$$

The solvent-mediated force for tip height H is obtained by differentiating the free energy with respect to the tip height as follows:

$$F_H = -\frac{E_{H+\Delta H} - E_H}{\Delta H}. \quad (14)$$

The temperature of the entire system and the number density of the water molecules are set at 300 K and 0.0334 Å^{-3}, respectively.

D. Scan line and scan area

Force-distance curves along the z axis and force maps in the x-z plane as shown in Fig. 4 are obtained by the numerical calculations mentioned above. For the calculations of the force-distance curve, forces are obtained in the distance range from 2.0 Å to 15.0 Å at 0.25 Å intervals. For the simulation of x-z plane force map, the scan area is chosen as a 16.0×3.5 Å^2 rectangle whose shorter side lies from 2.5 Å to 6.0 Å of the z axis. The pixel size is chosen as 0.5×0.25 Å^2. Due to the symmetry of the tip and the surfaces, mirror images of calculated force maps can be duplicated as shown in Fig. 4. Images shown in Sec. III include the mirror images.

III. RESULTS

A. Force curves

At first, as a reference, force curves due to only the direct interactions V_{TS} [Eq. (3)] between the tip and the sample surface, namely the interaction in vacuum without water molecules are shown in Fig. 5. Three kinds of force curves are obtained. Here, for later convenience, combinations of the tip and the surface charging patterns are classified into the following three groups based on the types of the calculated force curves. The first group, group A, is made up of the combinations of T0S0, T0S1, T0S2, T1S0, and T2S0. The second group, group B, is made up of the combinations

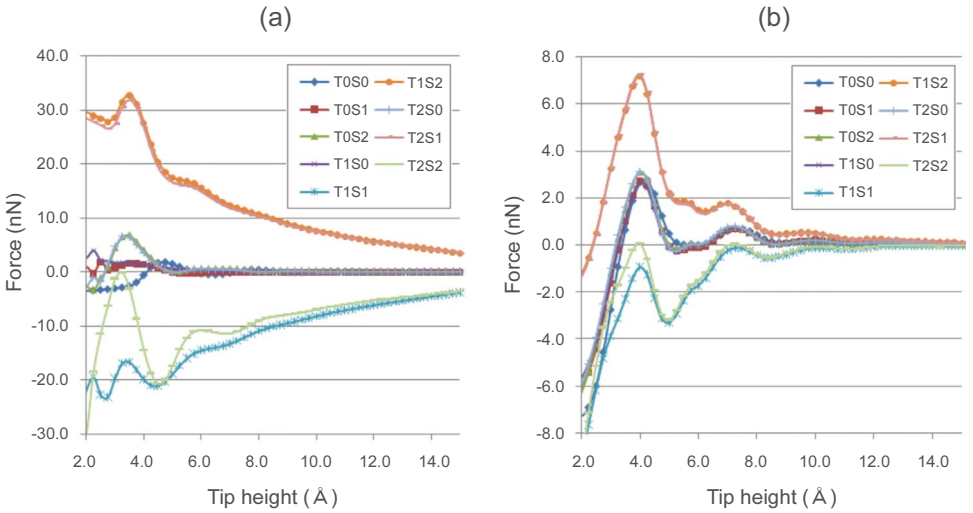

FIG. 6. (Color online) Force curves in water (a) and (b) do not include the direct interactions and were obtained by the 3D-RISM and the RISM theories, respectively.

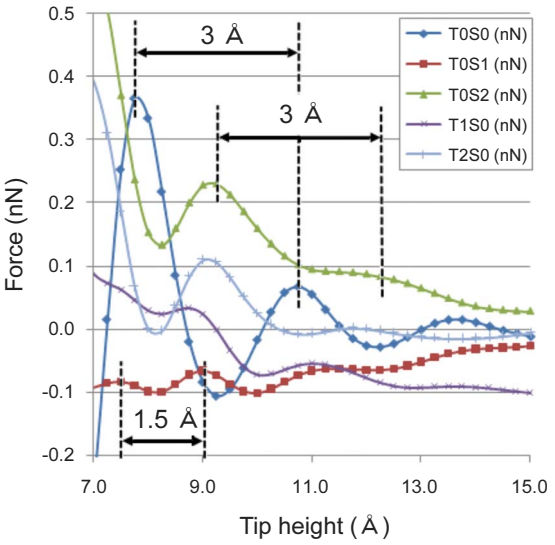

FIG. 7. (Color online) The magnified image of the force curves in water of group A obtained by the 3D-RISM theory. The forces do not include the direct interactions.

of T1S1 and T2S2. The third group, group C, is made up of the combinations of T1S2 and T2S1. Considering the potential parameters for the direct interactions, it is obvious that the force curves in the same group are exactly the same as each other. The force curve of group A reflects only the Lennard-Jones potentials. The force curve of group B reveals a strong repulsive force region by the effect of the electrostatic interactions, while the force curve of group C shows a strong attractive region.

The force curves in water obtained by the 3D-RISM theory and those obtained by the RISM theory are shown in Figs. 6(a) and 6(b), respectively. Force curves represent only the contribution to the force by the water molecules. Namely, the direct interactions between the tips and the sample surfaces shown in Fig. 5 are not included in the force curves. Figure 7 is magnified force curves of group A obtained by the 3D-RISM theory. Oscillations of force with the tip height can be seen on both the force curves by the 3D-RISM theory and the RISM theory.

The origin of the force oscillation is the oscillatory features of the density distribution of water molecules near the interface known from various experiments.[67] The oscillatory features of the water density represent the time average of water molecules moving much faster than the tip. Namely, the features are not disturbed by the motion of the tip and depend only on the position of the tip. The period of the oscillation 3.0 Å calculated in this work is somewhat longer than the actually observed period of 2.526 ± 0.482 Å.[67] It is not difficult to reproduce the experimental period by tuning the potential parameter, but we did not perform such tuning because our purpose is to deduce essential features of the water mediated forces.

For the case using the 3D-RISM theory [Figs. 6(a) and 7], the force curves in the same charging pattern group, i.e., within either group A, B, or C, have different features from each other unlike the force curves of the direct interaction in vacuum (Fig. 5); the periods and the phases of the force curve oscillation are different from each other. For example, the period for T0S1 is 1.5 Å while those for T0S0 and T0S2 are 3 Å as shown in Fig. 7. The phase for T0S0 is shifted from that for T0S2 by 1.5 Å, i.e., half the period. Like in vacuum, the force curves for the charging patterns of group B are shifted to the opposite direction to those in the group C. Interestingly, however, the direction of the shift in water are reversed compared with that in vacuum. Namely, the force curves of group B (C) shift to the repulsive (attractive) side in vacuum, but shift to the attractive (repulsive) side by the water effect, as is seen in the calculated results of Fig. 6(a) by the 3D-RISM theory.

For the case using the RISM theory [Fig. 6(b)], the differences among the force curves in the same charging pattern groups are not as large as those using the 3D-RISM theory. Unlike the 3D-RISM theory, the periods and the phases of the nine force curves are almost the same as each other. Absolute values of forces by the RISM theory are smaller than those by the 3D-RISM theory.

Water density distributions at the gap between a tip and a surface govern the free energies and the forces. The deviation of the water density distribution from the bulk is large and considerably far reaching beyond 1nm as can be seen in Figs. 13 and 14.

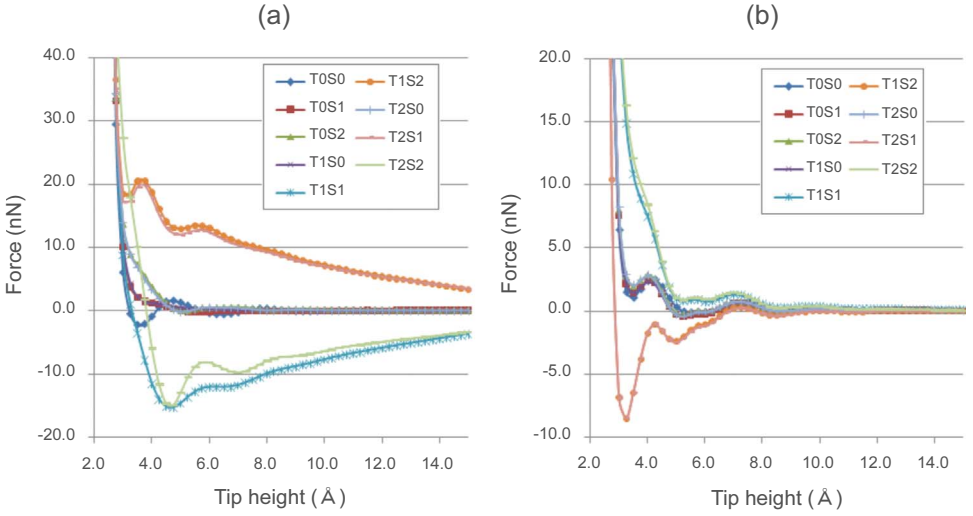

FIG. 8. (Color online) Force curves in water (a) and (b) were obtained by the 3D-RISM theory and the RISM theory, respectively. The direct interactions between the tips and the surfaces are included in the force curves.

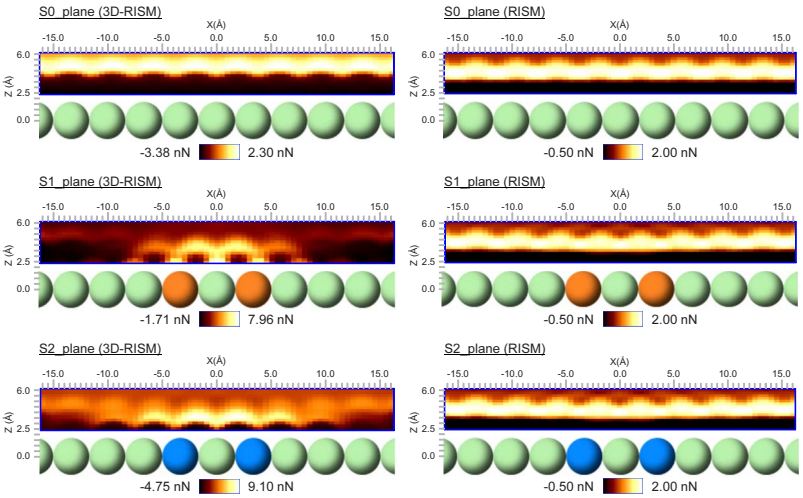

FIG. 9. (Color online) Maps of water mediated forces on the plane surfaces obtained by the 3D-RISM theory (left) and the RISM theory (right) in the yellow colored and the blue colored areas in the *x*-*z* plane shown in Fig. 4 using the tip of charging pattern 0.

As will be also discussed in Sec. III B, the density distribution of the water molecules near the surface is more adequately described by the 3D-RISM theory than the RISM theory. This is because, in the RISM theory, the local density distribution near the surface tends to be averaged out with that in the bulk. This is the reason why the forces obtained by the RISM theory Fig. 6(b) are smaller than the ones obtained by the 3D-RISM theory Fig. 6(a), and its range is much shorter than the one by the 3D-RISM theory.

The total force curves which are obtained by simply summed up the force curves Figs. 5 and 6 are shown in Figs. 8(a) and 8(b) for the 3D-RISM theory and the RISM theory, respectively. The calculation by the 3D-RISM theory indicates the water mediated force is of long range, and the repulsive potential of the group B in vacuum is changed to be attractive, and the attractive potential of the group C in vacuum is changed to be repulsive.

Although the absolute values of the forces by water molecules are calculated to be larger than the direct interactions based on the 3D-RISM theory, it is not essential because the absolute values of the direct interactions depends on the tip model and will be larger if a more realistic larger tip is used.

B. Force maps

The force maps of the six surfaces, S0_plane, S1_plane, S2_plane, S0_pit, S1_pit, and S2_pit with the tip T0 of the charging pattern 0 in water are obtained by the 3D-RISM theory and the RISM theory. They are shown in the left and right columns of Fig. 9, respectively. The force maps are constructed only by the water mediated forces and do not include the direct interactions between the tip and the surfaces.

Differences in charging patterns are strongly reflected on the three force maps of the plane surfaces obtained by the 3D-RISM theory. In the force maps of S1_plane and S2_plane, characteristic patterns showing local stronger repulsive force regions are seen above the charged atoms, while only a uniformly repeated pattern is seen in the force map of S0_plane. The three force maps of the pit surfaces, S0_pit, S1_pit, and S2_pit, obtained by the 3D-RISM theory do not show noticeable difference each other. Namely, similar shaped patterns of stronger repulsive force region, consisted of isolated bright (repulsive) island and weaker gap region to the remaining bright belt, are seen above the pit.

There is no significant difference among the three force maps of the plane surfaces obtained by the RISM theory, unlike those obtained by the 3D-RISM theory. Similar uniformly repeated patterns are seen in all the three force maps. For the force maps of the pit surfaces, there is no significant difference among the three; similar shaped repulsive force regions are seen above the pit. This is the same feature as the force maps obtained by the 3D-RISM theory, but the pattern

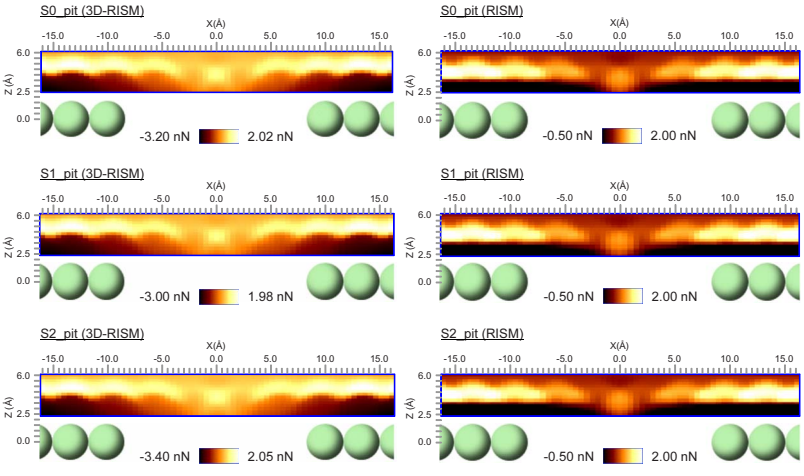

FIG. 10. (Color online) Maps of water mediated forces on the pit surfaces obtained by the 3D-RISM theory (left) and the RISM theory (right) in the yellow colored and the blue colored areas in the *x*-*z* plane shown in Fig. 4 using the tip of charging pattern 0.

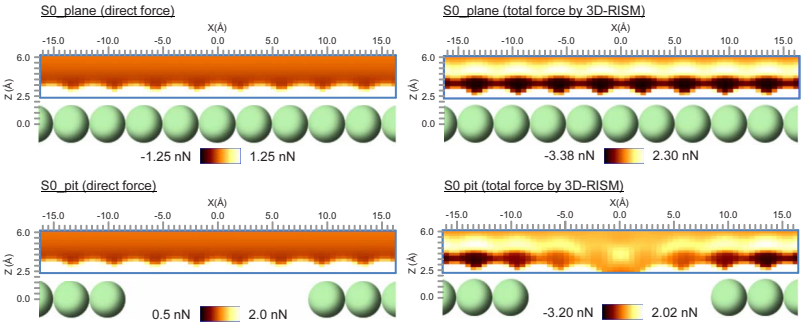

FIG. 11. (Color online) Maps of direct forces (left) and their combinations with the water mediated forces obtained by the 3D-RISM theory (right) in the yellow colored and the blue colored areas in the x-z plane shown in Fig. 4 using the tip of T0.

above the pit becomes less bright compared with the distant region from the pit.

Force maps for the two surfaces without the charge, S0_plane and S0_pit, and the tip without the charge, T0, are calculated by the 3D-RISM theory, and are shown for the case in vacuum and in water, respectively, in Fig. 11. Unlike the force maps in water, there is no repulsive force region above the pit in the force maps of the direct interactions in vacuum. Microscopic structures of the surfaces are reflected on the force maps from much more distant regions from the surfaces in the water mediated forces than the case of the direct forces in vacuum. This can be clearly seen in water mediated force maps in the right column of Fig. 11.

IV. DISCUSSIONS

A. Distributions of oxygen and hydrogen atoms of water

For the analyses and physical interpretation of the main features of the force curves and the force maps presented in the previous section, density distributions of the oxygen and the hydrogen atoms of water molecules in the three-dimensional real space around the tip and sample surface are obtained by the 3D-RISM theory. Density distributions for the three surfaces with the respective charging patterns are calculated and are shown in the vertical cross sections including the red lines in Fig. 12. Density distributions around the plane surfaces, the tips and the pit surfaces are shown in Figs. 13–15, respectively.

The densities of the atoms are represented by the difference values from the mean densities of the atoms in the bulk water. The difference values are normalized with respect to the mean densities. Namely, the difference values of −1.0, 0.0, and 1.0 correspond to the zero density, the mean densities and twice the mean densities, respectively. The density distributions are colored based on the difference values. For the map of the oxygen (hydrogen) atom, the regions with the difference values more than 0.0, namely, the regions with higher densities than the mean density, are colored blue (red). The regions with the difference values less than 0.0, namely, the regions with lower densities than the mean density are colored gray.

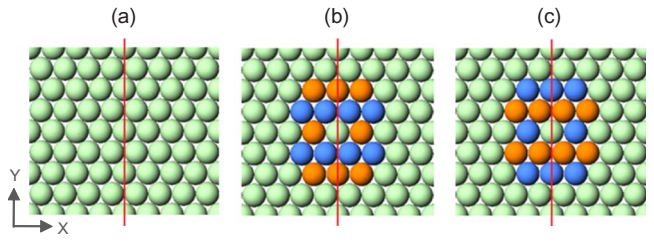

FIG. 12. (Color online) Red lines in (a), (b), and (c) are the cross-sections, $X=0$ Å, to obtain density distributions of water for charging patterns 0, 1, and 2, respectively.

In the density distributions above the S0_plane [Figs. 13(a) and 13(b)], layered structures with the interlayer spacing of 3.0 Å parallel to the surface are seen. The layered structures consist of patterns repeated uniformly along the y axis with the same period as that of the surface structure. Similar layered structures are seen in the regions of $Y=-20$ Å to −10 Å and $Y=10$ Å to 20 Å above S1_plane [Figs. 13(c) and 13(d)] and in the regions $Y=-20$ Å to −7 Å and $Y=7$ Å to 20 Å above S2_plane [Figs. 13(e) and 13(f)]. In the regions above the charged atoms of S1_plane, $Y=-10$ Å to 10 Å, a pattern consisting of two types of layered structure are seen. The first type of layered structure is seen in the regions of $Y=3$ Å to 10 Å and $Y=-10$ Å to −3 Å. And the second type is seen in the region of $Y=-3$ Å to 3 Å. The interlayer spacing for the both type is 3 Å. The layers of the first type are shifted from those of the second type by half the interlayer spacing, 1.5 Å, along the z axis. In the regions above the charged atoms of S2_plane, $Y=-7$ Å to 7 Å, a layered structure is formed. The interlayer spacing of the layered structure is 3 Å and the layers are shifted from the layers in the other region by half the interlayer spacing, 1.5 Å, along the z axis. For all the cases, the contrasts of the density distribution of oxygen and hydrogen atoms in water show a larger variation nearer to the surfaces.

The features of the density distributions of water molecules around the three isolated tips from the surface, T0, T1, and T2 are similar to those above the three plane surfaces, S0_plane, S1_plane and S2_plane, respectively, as shown in Fig. 14.

The features of the density distributions of water molecules just above the third layers of the three pit surfaces, S0_pit, S1_pit, and S2_pit, are similar to those just above the three plane surfaces, S0_plane, S1_plane, and S2_plane, respectively, as shown in Fig. 15. Around the entrances of the pits, the features of the density distributions of the three surfaces are similar to each other; they follow the peripheral shape of the pit wall.

B. Force curves and density distributions of water

The periods, the phases and the amplitudes of the force curve oscillations obtained by the 3D-RISM theory [Figs.

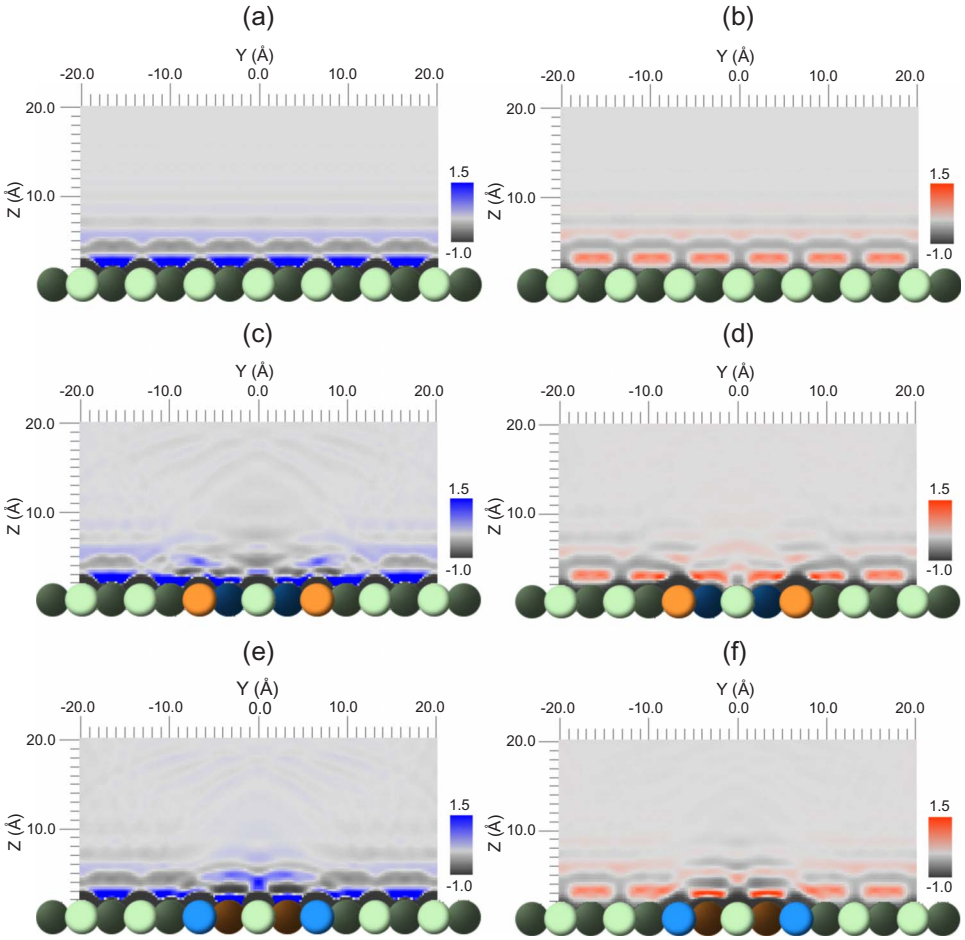

FIG. 13. (Color online) Distributions of the oxygen and the hydrogen atoms of water on the plane surface isolated in water. The surfaces and the elements of the water atom of 6 distributions are (a): S0_plane-O, (b): S0_plane-H, (c): S1_plane-O, (d): S1_plane-H, (e): S2_plane-O, and (f): S2_plane-H. Bright colored atoms are centered on the planes shown as the red lines in Fig. 12. Dark colored atoms are separated from the plane by half the distance between two adjacent atoms.

6(a) and 6(c)] are related to the patterns of the layered structures of density distribution of water molecules around the tips and the surfaces [Figs. 13 and 14]. The force oscillation periods of 3.0 Å for T0S0 and T0S2 are the same as the interlayer spacing of the layered structure of water above S0_plane and that above the charged atoms of S2_plane. The period of 1.5 Å for T0S1 (Fig. 6) corresponds to the fact that the two types of layered structure existing above the charged atoms of S1_plane [Figs. 13(c) and 13(d)], which have the same interlayer spacing of 3 Å, are shifted by 1.5 Å from each other. The shift of the peak distance of 1.5 Å between the force oscillation for T0S0 and that for T0S2 (Fig. 6) corresponds to the shift between the layered structure above S0_plane and that above the charged atom region of S2_plane as seen in Figs. 13(a) and 13(c). As a general feature of the force curve, we find that the nearer the tip to the surfaces, the larger the amplitudes of the oscillation of force curves. This corresponds to the fact that the contrasts of water density oscillation are larger nearer to the surfaces.

For further understanding of the relations between the water mediated forces and the density distributions of water, relative free energies using the 3D-RISM theory are plotted with respect to the tip heights in Fig. 16. Here, the relative free energy at tip height H means the free energy at the tip height H, E_H calculated by Eq. (12), relative to the free energy when the tip is infinitely far from the surface, E_∞. The direct interactions between the tips and the surfaces, V_{TS}, are not included in the free energies.

At the tip heights of 11.5 and 10.0 Å, the relative free energy of T0S0 takes a local minimum and a local maximum, respectively [Fig. 16(b)]. Density distributions of the oxygen and the hydrogen atoms of water around T0S0 at the tip height of 11.5 Å are shown in Figs. 17(a) and 17(b) and those at the tip height of 10.0 Å are shown in Figs. 17(c) and 17(d). In Figs. 17(a) and 17(b), a water layer is formed about 5.5–6.0 Å above the surface, namely, 6.0–5.5 Å below the tip. The layer is flat and spread from Y=−20–20 Å. In Figs. 17(c) and 17(d), although a similar water layer is formed about 5.5–6.0 Å above the surface region distant from the tip, the layer disappears below the tip, namely, in the region of Y=−6–6 Å and 4.5–4.0 Å below the tip. As shown in Figs. 13(a) and 13(b), a water layer is formed about 5.5–6.0 Å above the isolated S0_plane in water. As shown in Figs. 14(a) and 14(b), a water layer is formed about 6.0–5.5 Å below the isolated T0 in water, but no layer is formed about 4.5–4.0 Å below the tip. Namely, the relative

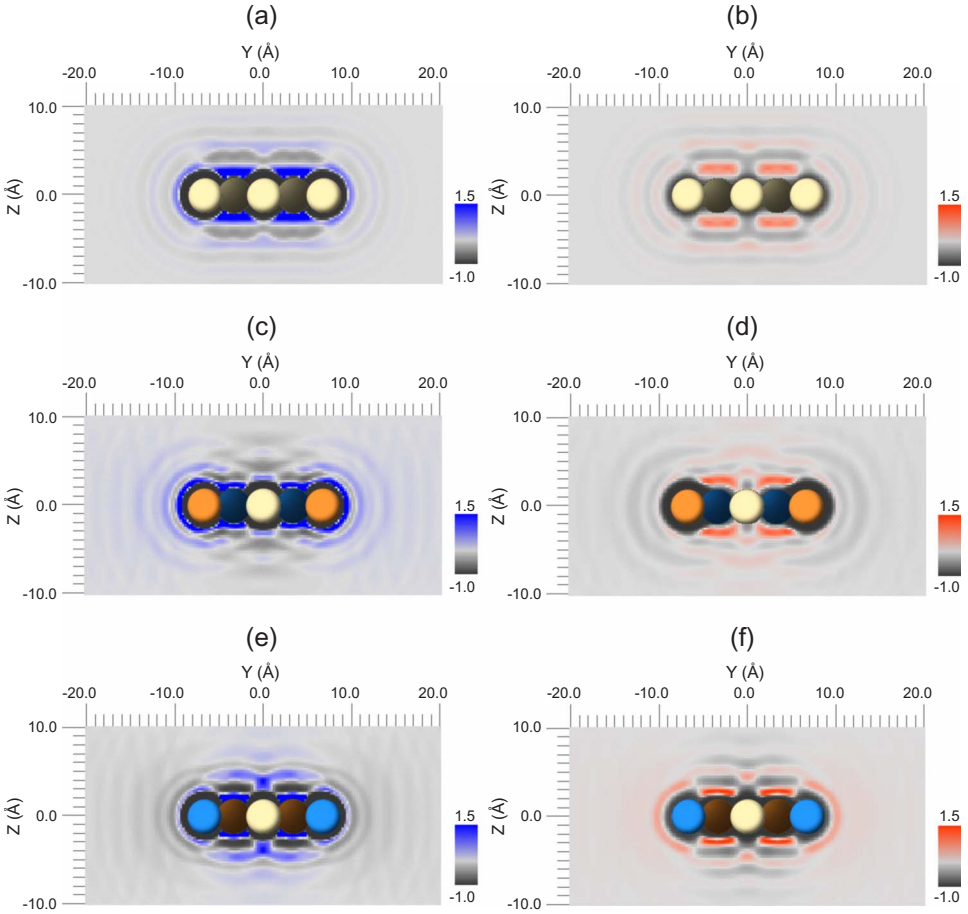

FIG. 14. (Color online) Distributions of the oxygen and the hydrogen atoms of water around the tip isolated in water. The charging patterns of the tip and the elements of the water atom of 6 distributions are (a): T0-O, (b): T0-H, (c): T1-O, (d): T1-H, (e): T2-O, and (f): T2-H. Bright colored atoms are centered on the planes shown as the red lines in Fig. 12. Dark colored atoms are separated from the plane by half the distance between two adjacent atoms.

free energy takes a local minimum and a local maximum when the overlapping of the water density distribution around the tip alone and that around the surface alone interferes positively or negatively, respectively. From the above, it is generally concluded that there is a negative correlation between the relative free energy and the constructive interference of water density distributions around the tip and the surface.

As explained in Sec. IV A, the force curves for the groups B and C in water are shifted oppositely to those in vacuum. Namely, the force curves for groups B and C shift to the attractive and the repulsive directions, respectively [Figs. 6(a) and 6(b)], while they are shifted to the repulsive and the attractive side, respectively, in vacuum (Fig. 5). This feature can also be explained by the negative correlation between the relative free energy and the constructive interference of water density distributions around the tip alone and the surface alone. For example, as shown in Fig. 16(a), the relative free energies of T1S1 and T1S2 are shifted to the negative and the positive regions, respectively. The oxygen atom density above the isolated S1 shown in Fig. 13(c) is less than the mean density and coincides with that under the isolated T1 shown in Fig. 14(c). On the other hand, the oxygen atom density above the isolated S2 shown in Fig. 13(e) shows strongly accumulated regions, which are remarkably different from those under the isolated T1.

From the above discussions, it has been clarified that the water density distributions localized between a tip and a surface dominate the free energy and the force. Generally, localized water density distributions are more precisely reflected in the calculation by the 3D-RISM theory using the three dimensional coordinate than the RISM theory only using the radial coordinate averaging over the orientation. This understanding is consistent with the fact that the forces obtained by the 3D-RISM theory are larger and reach to farer region than the ones obtained by the RISM theory as shown in Fig. 6.

C. Force maps and density distributions of water

As explained in sub, the significant differences are seen in the force maps (Fig. 9) for the three plane surfaces, S0_plane, S1_plane and S2_plane obtained by the 3D-RISM, unlike those obtained by the RISM theory. The appearance of the differences is consistent with the remarkably different density distributions of water molecules above the three plane surfaces, as shown in Fig. 13. The different distributions of the water molecules above the three charging pattern

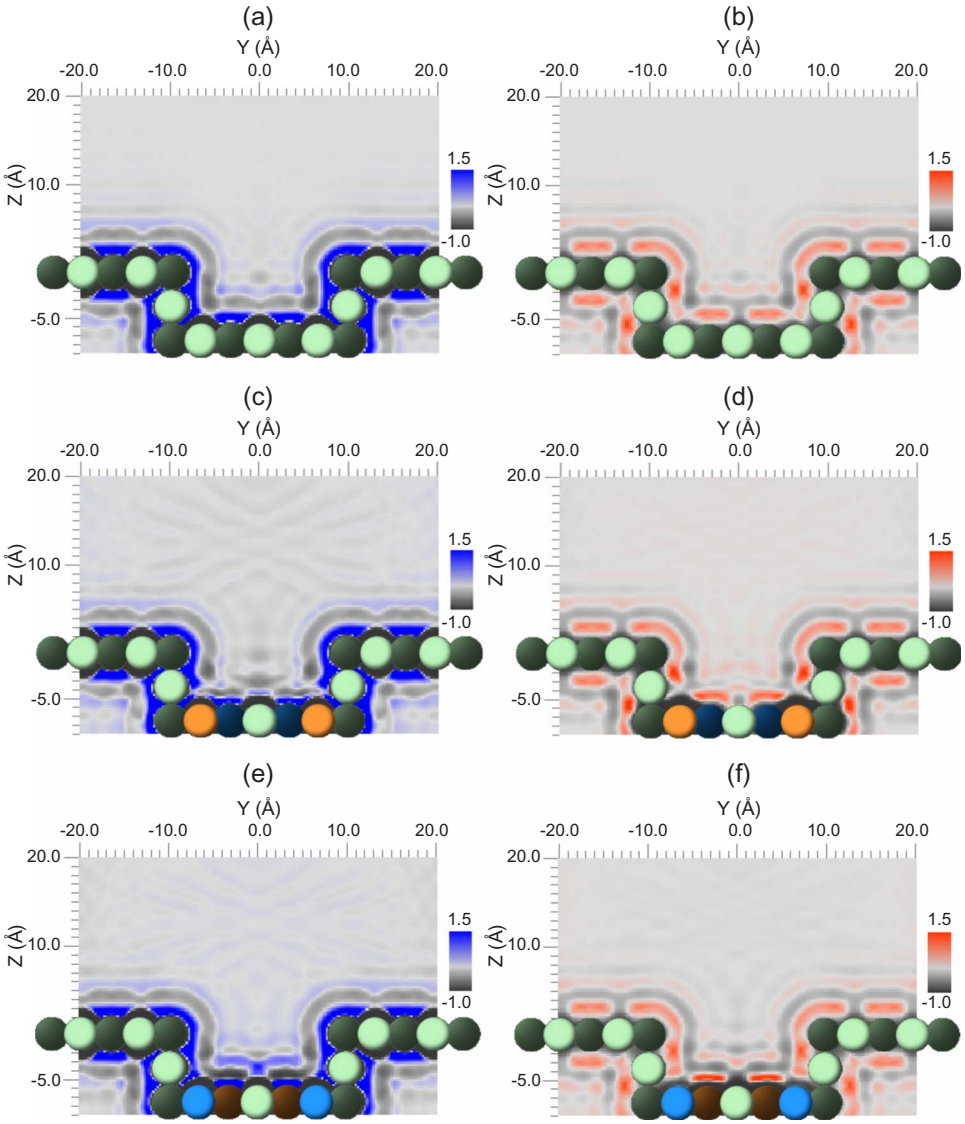

FIG. 15. (Color online) Distributions of the oxygen and the hydrogen atoms of water on the pit surface isolated in water. The charging patterns of the pit surface and the elements of the water atom of 6 distributions are (a): S0-O, (b): S0-H, (c): S1-O, (d): S1-H, (e): S2-O, and (f): S2-H. Bright colored atoms are centered on the planes shown as the red lines in Fig. 12. Dark colored atoms are separated from the plane by half the distance between two adjacent atoms.

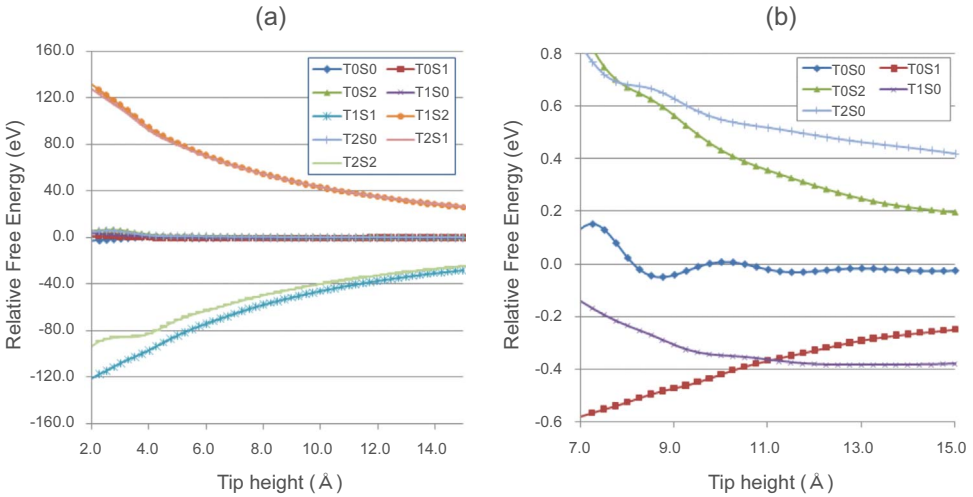

FIG. 16. (Color online) The relative free energies obtained by the 3D-RISM theory. (b) is the magnified images for charging pattern group A.

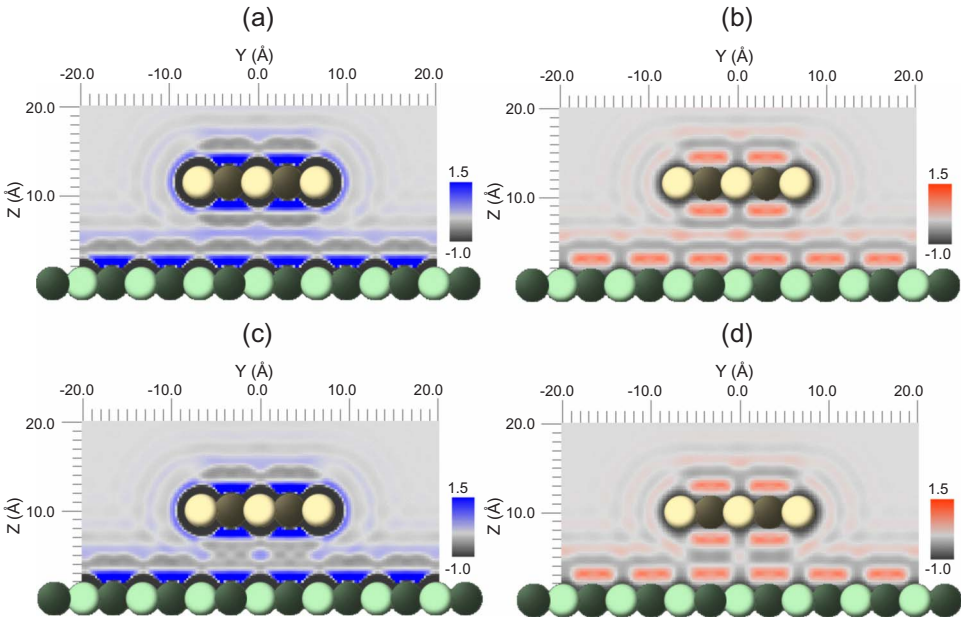

FIG. 17. (Color online) Density distributions of the oxygen and the hydrogen atoms of water around T0S0 for the tip heights of 11.5 and 10.0 Å. The tip heights and the elements of the water atom of the four density distributions are (a): 11.5 Å-O, (b): 11.5 Å-H, (c): 10.0 Å-O, and (d): 10.0 Å-H. Bright colored atoms are centered on the planes shown as the red lines in Fig. 12. Dark colored atoms are separated from the plane by half the distance between two adjacent atoms.

cannot be reproduced and impossible to be reflected in the force maps by the RISM theory, because the total correlation functions, $h(r)$, and the direct correlation functions, $c(r)$, obtained within the approximation of the RISM theory depend only on the distances between atoms.

As explained in Sec. IV B, localized repulsive force regions are seen just above the pits for three pit surfaces (Fig. 10). In the force map of S0_pit (3D-RISM), the localized repulsive force region appears between the tip heights of 3.25–5.0 Å along the line $X=0.0$. The reason of the appearance of such localized repulsive region is explained as follows. This pattern indicates that the free energy takes a local minimum and a local maximum at the tip heights of 5.0–3.25 Å, respectively, when it goes down along the vertical line through the point $X=0.0$ (center of the figure). Density distributions of water at the two tip heights are shown in Fig. 18. For the tip height of 5.0 Å, a water layer is formed in the region between two atoms ① and ② of Fig. 18(a). In the corresponding regions around the isolated T0 [Figs. 14(a) and 14(b)] and the isolated S0_pit [Figs. 15(a) and 15(b)], large densities of water molecules are seen. Namely, a positive overlap of the two large water densities appears for the whole tip-surface system, which results in a local minimum for the tip heights of 5.0 Å. On the other hand, the overlap is destructive leading to a local maximum of the free energy at the tip height of 3.25 Å; the water layer completely disappears as show in Figs. 18(c) and 18(d). This explains a strong repulsive spot at the tip heights from 3.5–5.0 Å above the pit center. Because the features of the water density distributions around the pit entrances of the two other pit surfaces, S1_pit and S2_pit, are similar to S0_pit as explained in Sec. IV A, the similar repulsive force regions are also seen for S1_pit and S2_pit.

As discussed so far, the water mediated forces strongly depend on the constructive or destructive interference of the overlap of the water density distributions around isolated systems of tip and surface. As seen in Fig. 11, structures of the surfaces can be detected by the tip force in water from much farther regions than the case in vacuum. This is because the atomic structures of the surfaces are reflected in the density distributions of water molecules, shown in Figs. 13 and 15, farther above the surfaces than the largest distances where the atomic structure are reflected in the direct forces.

V. SUMMARY

In this paper, the force curves and the force maps of AFM measurements in water have been theoretically simulated for systems consisting of hypothetical structures of the tip and the surfaces made up of hypothetical atoms using the 3D-RISM theory. The density distributions of water molecules around the tip alone and the surfaces alone in water have been also obtained for the reference using the 3D-RISM theory.

We have reached a general conclusion that there is a negative correlation between the relative free energy of the system in water and the constructive overlapping of the density distribution of water molecules around the isolated tip and the isolated surface. From this conclusion, specific behaviors of the force oscillation which is felt by a tip on a sample surface is correlated with the detailed shape and interlayer spacing of the oscillatory structures of the density distribution of water molecules around the isolated tip and the surface. An interesting phenomenon found in the present work is that the direction of the water mediated forces for a charged tip on a charged surface is opposite to the directions

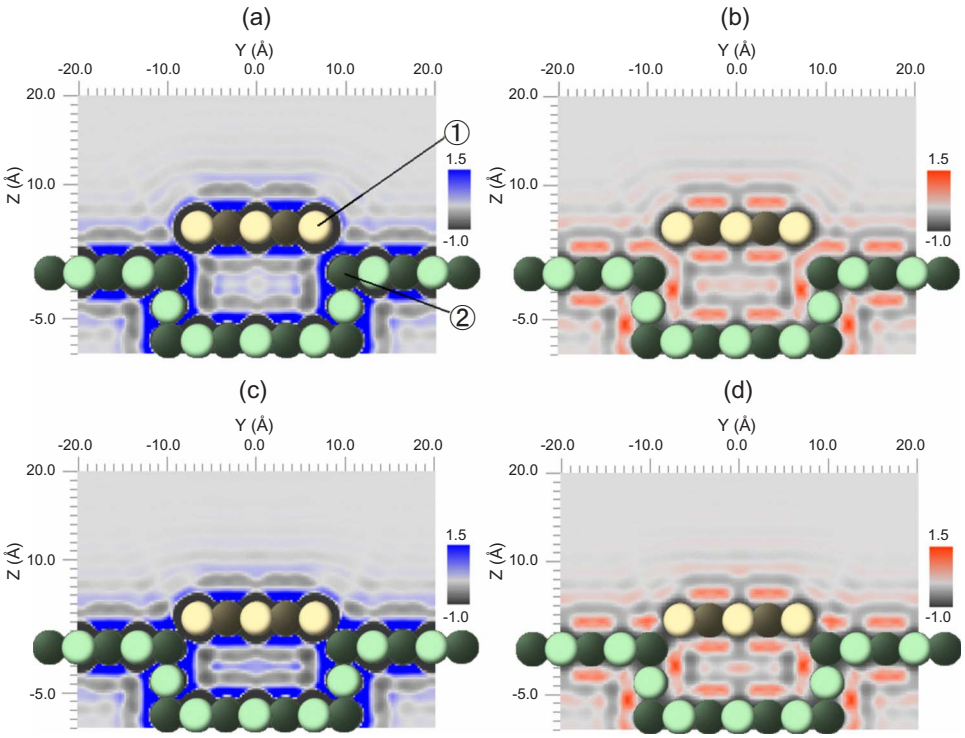

FIG. 18. (Color online) Distributions of the oxygen and the hydrogen atoms of water around T0S0_pit for the tip heights of 5.0 and 3.25 Å. The tip heights and the elements of the water atom are (a): 5.0 Å-O, (b): 5.0 Å-H, (c): 3.25 Å-O, and (d): 3.25 Å-H. Bright colored atoms are centered on the planes shown as the red lines in Fig. 12. Dark colored atoms are separated from the plane by half the distance between two adjacent atoms.

of the direct forces in vacuum. The features of the force maps in the nanostructured surface in water, as well as the effect of the local charging have been clarified and discussed in relation to the density distribution pattern of water molecules.

We also demonstrated the 3D-RISM theory is much more accurate for AFM simulations in water than the RISM theory. Some of the features of the force curves and the force maps obtained by the 3D-RISM theory cannot be seen in the simulation results by the RISM theory.

ACKNOWLEDGMENTS

This study was supported in part by the Japan Science and Technology Agency (JST) program "Development of System and Technology for Advanced Measurement and Analysis."

*Corresponding author. Advance Soft Corporation, 1-9-20 Akasaka, Minato-ku, Tokyo 107-0052, Japan; http://www.cms.nano.waseda.ac.jp; harada@advancesoft.jp

[1] G. Binnig, C. F. Quate, and C. Gerber, Phys. Rev. Lett. **56**, 930 (1986).
[2] N. Oyabu, O. Custance, I. Yi, Y. Sugawara, and S. Morita, Phys. Rev. Lett. **90**, 176102 (2003).
[3] N. Oyabu, Y. Sugimoto, M. Abe, O. Custance, and S. Morita, Nanotechnology **16**, S112 (2005).
[4] Y. Sugimoto, M. Abe, S. Hirayama, N. Oyabu, O. Custance, and S. Morita, Nature Mater. **4**, 156 (2005).
[5] C. Loppacher, M. Bammerlin, M. Guggisberg, F. Battiston, R. Bennewitz, S. Rast, A. Baratoff, E. Meyer, and H. Guntherodt, Appl. Surf. Sci. **140**, 287 (1999).
[6] N. Sasaki and M. Tsukada, Jpn. J. Appl. Phys. **39**, L1334 (2000).
[7] N. Sasaki and M. Tsukada, Phys. Rev. B **52**, 8471 (1995).
[8] N. Sasaki and M. Tsukada, Jpn. J. Appl. Phys. **38**, 192 (1999).
[9] N. Sasaki, H. Aizawa, and M. Tsukada, Jpn. J. Appl. Phys. **39**, L174 (2000).
[10] N. Sasaki, S. Watanabe, and M. Tsukada, Phys. Rev. Lett. **88**, 046106 (2002).
[11] N. Sasaki, K. Kobayashi, and M. Tsukada, Phys. Rev. B **54**, 2138 (1996).
[12] N. Sasaki, M. Tsukada, S. Fujisawa, Y. Sugawara, S. Morita, and K. Kobayashi, Phys. Rev. B **57**, 3785 (1998).
[13] M. Harada, M. Tsukada, and N. Sasaki, e-J. Surf. Sci. Nanotechnol. **5**, 126 (2007).
[14] M. Harada and M. Tsukada, Phys. Rev. B **77**, 205435 (2008).
[15] A. S. Foster, O. H. Pakarinen, J. M. Airaksinen, J. D. Gale, and R. M. Nieminen, Phys. Rev. B **68**, 195410 (2003).
[16] R. Hoffmann, L. N. Kantorovich, A. Baratoff, H. J. Hug, and H.-J. Güntherodt, Phys. Rev. Lett. **92**, 146103 (2004).
[17] G. H. Enevoldsen, H. P. Pinto, A. S. Foster, M. C. R. Jensen, W. A. Hofer, B. Hammer, J. V. Lauritsen, and F. Besenbacher, Phys.

Rev. Lett. **102**, 136103 (2009).
[18] R. Bechstein, C. González, J. Schütte, P. Jelínek, R. Pérez, and A. Kühnle, Nanotechnology **20**, 505703 (2009).
[19] H. P. Pinto, G. H. Enevoldsen, F. Besenbacher, J. V. Lauritsen, and A. S. Foster, Nanotechnology **20**, 264020 (2009).
[20] A. S. Foster, C. Barth, A. L. Shluger, and M. Reichling, Phys. Rev. Lett. **86**, 2373 (2001).
[21] R. Pérez, M. C. Payne, I. Štich, and K. Terakura, Phys. Rev. Lett. **78**, 678 (1997).
[22] S. H. Ke, T. Uda, I. Štich, and K. Terakura, Phys. Rev. B **63**, 245323 (2001).
[23] Y. Sugimoto, O. Custance, S. Morita, M. Abe, P. Pou, P. Jelinek, and R. Pérez, Phys. Rev. B **73**, 205329 (2006).
[24] S. Sadewasser, P. Jelinek, C.-K. Fang, O. Custance, Y. Yamada, Y. Sugimoto, M. Abe, and S. Morita, Phys. Rev. Lett. **103**, 266103 (2009).
[25] V. Caciuc and H. Hölscher, Nanotechnology **20**, 264006 (2009).
[26] Y. Sugimoto, P. Pou, M. Abe, P. Jelinek, R. Pérez, S. Morita, and Ó. Custance, Nature (London) **446**, 64 (2007).
[27] C. Lazo, V. Caciuc, H. Hölscher, and S. Heinze, Phys. Rev. B **78**, 214416 (2008).
[28] Y. Sugimoto, P. Pou, O. Custance, P. Jelinek, M. Abe, R. Perez, and S. Morita, Science **322**, 413 (2008).
[29] P. Dieška and I. Štich, Phys. Rev. B **79**, 125431 (2009).
[30] N. Martsinovich and L. Kantorovich, Nanotechnology **20**, 135706 (2009).
[31] N. Atodiresei, V. Caciuc, S. Blügel, and H. Hölscher, Phys. Rev. B **77**, 153408 (2008).
[32] Y. Sugimoto, P. Jelinek, P. Pou, M. Abe, S. Morita, R. Perez, and O. Custance, Phys. Rev. Lett. **98**, 106104 (2007).
[33] T. Fukuma, M. J. Higgins, and S. P. Jarvis, Phys. Rev. Lett. **98**, 106101 (2007).
[34] T. Fukuma, M. Kimura, K. Kobayashi, K. Matsushige, and H. Yamada, Rev. Sci. Instrum. **76**, 053704 (2005).
[35] J. Hogan, Nature (London) **440**, 14 (2006).
[36] T. Fukuma, K. Kobayashi, K. Matsushige, and H. Yamada, Appl. Phys. Lett. **86**, 193108 (2005).
[37] T. Fukuma, K. Kobayashi, K. Matsushige, and H. Yamada, Appl. Phys. Lett. **87**, 034101 (2005).
[38] B. Hoogenboom, H. Hug, Y. Pellmont, S. Martin, P. Frederix, D. Fotiadis, and A. Engel, Appl. Phys. Lett. **88**, 193109 (2006).
[39] M. Sampoli, G. Ruocco, and F. Sette, Phys. Rev. Lett. **79**, 1678 (1997).
[40] G. Monaco, A. Cunsolo, G. Ruocco, and F. Sette, Phys. Rev. E **60**, 5505 (1999).
[41] S. Santucci, S. Di Fonzo, and C. Masciovecchio, J. Electron Spectrosc. Relat. Phenom. **144-147**, 941 (2005).
[42] W. Press, S. Teukolsky, W. Vetterling, and B. Flannery, *Numerical Recipes in C* (Cambridge University Press, Cambridge, England, 1992).
[43] J. Tomasi and M. Persico, Chem. Rev. **94**, 2027 (1994).
[44] C. Cramer and D. Truhlar, Chem. Rev. **99**, 2161 (1999).
[45] B. Guillot, J. Mol. Liq. **101**, 219 (2002).
[46] J. Rivera, M. Predota, A. Chialvo, and P. Cummings, Chem. Phys. Lett. **357**, 189 (2002).
[47] D. Price and C. Brooks III, J. Chem. Phys. **121**, 10096 (2004).
[48] H. Horn, W. Swope, J. Pitera, J. Madura, T. Dick, G. Hura, and T. Head-Gordon, J. Chem. Phys. **120**, 9665 (2004).
[49] W. L. Jorgensen and J. Tirado-Rives, Proc. Natl. Acad. Sci. **102**, 6665 (2005).
[50] F. Hirata, *Molecular Theory of Solvation* (Kluwer, Dordrecht, 2003).
[51] D. Chandler and H. Andersen, J. Chem. Phys. **57**, 1930 (1972).
[52] D. Chandler, J. Chem. Phys. **59**, 2742 (1973).
[53] F. Hirata and P. J. Rossky, Chem. Phys. Lett. **83**, 329 (1981).
[54] F. Hirata, B. Pettitt, and P. Rossky, J. Chem. Phys. **77**, 509 (1982).
[55] F. Hirata, P. Rossky, and B. Pettitt, J. Chem. Phys. **78**, 4133 (1983).
[56] K. Koga, X. Zeng, and H. Tanaka, J. Chem. Phys. **106**, 9781 (1997).
[57] K. Koga and X. C. Zeng, Phys. Rev. Lett. **79**, 853 (1997).
[58] K. Koga and X. C. Zeng, Phys. Rev. B **60**, 14328 (1999).
[59] C. Cortis, P. Rossky, and R. Friesner, J. Chem. Phys. **107**, 6400 (1997).
[60] D. Beglov and B. Roux, J. Phys. Chem. B **101**, 7821 (1997).
[61] A. Kovalenko and F. Hirata, Chem. Phys. Lett. **290**, 237 (1998).
[62] A. Kovalenko and F. Hirata, J. Chem. Phys. **110**, 10095 (1999).
[63] A. Kovalenko and F. Hirata, J. Chem. Phys. **112**, 10391 (2000).
[64] A. Kovalenko and F. Hirata, Chem. Phys. Lett. **349**, 496 (2001).
[65] W. L. Jorgensen, J. Am. Chem. Soc. **103**, 335 (1981).
[66] B. Pettitt and P. Rossky, J. Chem. Phys. **77**, 1451 (1982).
[67] S. Jeffery, P. M. Hoffmann, J. B. Pethica, C. Ramanujan, H. Özgür Özer, and A. Oral, Phys. Rev. B **70**, 054114 (2004).